Mechanical and physical performance of carbon aerogel reinforced carbon fibre hierarchical composites

Sang Nguyen[a], David B. Anthony[a,b,c], Hui Qian[a,b,c], Chuntong Yue[b], Aryaman Singh[a], Alexander Bismarck[b], Milo S.P. Shaffer[c], Emile S. Greenhalgh[a]*

[a] *The Composites Centre,* [b] *Polymer and Composite Engineering Group, Department of Chemical Engineering,* [c]*Nanostructured Hierarchical Assemblies and Composites Group, Departments of Materials and Chemistry, Imperial College London, London SW7 2AZ, UK*

s.nguyen@imperial.ac.uk, d.anthony08@imperial.ac.uk, sherryqian@gmail.com, aryaman.asyousay@gmail.com, alexander.bismarck@univie.ac.at, m.shaffer@imperial.ac.uk,

*e.greenhalgh@imperial.ac.uk *(+44 (0)20 7594 5070)*

Abstract

Carbon aerogel (CAG) is a potential hierarchical reinforcement to improve the matrix-dominated mechanical properties of continuous carbon fibre reinforced polymer (CFRP) composites in both multifunctional and purely structural applications. When using CAG to reinforce a polyethylene glycol diglycidyl ether (PEGDGE) matrix, the interlaminar shear strength, compressive modulus and strength increased approximately four-fold, whilst the out-of-plane electrical conductivity increased by 118 %. These mechanical and electrical performance enhancements significantly improve the multifunctional efficiency of composite structural supercapacitors, which can offer weight savings in transport and other applications. However, CAG also has the potential to reinforce conventional continuous CF composites in *purely structural* contexts. Here, CAG reinforcement of *structural* epoxy resin composites marginally increased

compressive (1.4%) and tensile (2.7%) moduli respectively, but considerably reduced compressive, tensile and interlaminar shear strengths. Fractographic analysis shows that the reduced performance can be attributed to poor interfacial adhesion; in the future, alternative processing routes may resolve these issues to achieve advances in both moduli and strengths over conventional structural CFRPs.

Keywords: A. Carbon aerogel composites; B. Mechanical properties; D. Fractography

1. Introduction

The principal performance hurdle for widespread adoption of polymer matrix composites in transport applications has been their poor matrix- and interface-dominated mechanical performance, particularly under longitudinal compression, in-plane shear and through-thickness loading. These limitations also result in a susceptibility to defects and damage, which has had a profound effect on the cost of certification and ownership of composite components. Over the last three decades, there has been a concerted effort to address matrix-dominated failures; the most popular strategy has been the addition of toughening phases to the matrix [1]. Progress to date has generally required a compromise between improved delamination resistance and depressed longitudinal compression performance, since such softer toughened phases offer inferior lateral support to the compressed fibres. Furthermore, the pursuit of tougher matrix systems has led to an increased sensitivity to processing conditions and higher material costs, as well as a depression of desirable physical properties such as thermal and electrical conductivity. In addition, increasing the fracture energy of CFRP is more complicated than simply enhancing the toughness of the resin, since the strength of the fibre-matrix interface controls many of the relevant mechanisms. The critical matrix-dominated weaknesses of carbon fibre reinforced polymers (CFRPs) have

stimulated interest in a range of hierarchical composites [2], including both nanostructured matrices [7] and bi-continuous systems, which can effectively improve the intrinsic properties of the matrix. Nanocarbon-based systems have been developed to exploit carbon nanotubes (CNT) [2] and more recently graphene-related materials [3,4]; however, progress has been limited by the quality of the fillers available in bulk and the need for additional surface chemistry, as well as processing challenges associated with self-filtration and agglomeration of more concentrated nanoreinforcement dispersions within composite microstructures [6,7]. Alternative approaches, such as the direct grafting of CNTs to carbon fibres, are promising but can be hard to scale and offer limited loading fractions [5]. Nevertheless, these hierarchical composites have demonstrated the potential to be superior to those relying on mesoscale toughening strategies that disrupt the parent architecture, such as Z-pinning [8].

1.1 Background and objectives

Carbon aerogels (CAGs) are widely used for their high surface area and electrical conductivity, particularly in the context of electrochemical electrodes and devices. The most common variety are formed by condensation, stabilisation and subsequent carbonisation of resorcinol-formaldehyde (RF) mixtures, to yield a network microstructure of amorphous carbon [9]. Unfortunately, CAGs tend to shrink and fracture due to internal stresses during synthesis, limiting the production of larger monoliths. For this reason, CAG-polymer composites have been produced by adding ground monolith powders as a conventional matrix modifier with [10] and without structural fibres [11]. Small monolithic structures have also been back-filled with a matrix [12] to create a bi-continuous reinforcement phase.

The aerogel shrinkage can be reduced, and the microstructure maintained by minimising the effects of surface tension during drying, but processes such as freeze- or super-critical drying typically limit the size of the aerogel monolith produced. Instead, the addition of macroscopic fibres to the aerogel sol-gel phase can stabilize subsequent processing without other measures. There has been significant development in this area, addressing the poor robustness of aerogels, as highlighted in a recent review for silica aerogel-based systems [13]. The principle of stabilising CAG synthesis by including non-structural randomly aligned fibres, felts or mats is also established [10,14]. As aerogels are usually used to provide high surface area for supercapacitor electrodes, or to improve thermal properties [14], investigation and optimisation of mechanical properties has been rather sparse [15]; the maximum compression strength and compression modulus reported are around 11 MPa and 650 MPa, respectively [16].

Fibre-reinforced aerogels (i.e. two-component systems) have a low density, due to the porosity of the aerogel which limits their mechanical performance. To overcome this limitation, the aerogel pores may be back-filled with a polymer to produce a consolidated fibre-reinforced aerogel composite (i.e. three-component system) [17]. Work to date has used randomly-aligned short fibres with modest mechanical performance due to the poor fibre alignment along the loading axis and inefficient load transfer [17]. Guan *et al*. [17] measured a compressive strength and modulus of 126 MPa and 2 GPa, respectively, using randomly-aligned aramid fibres and a graphene oxide-reinforced CAG microstructure infused with epoxy.

Rather than attempting to improve aerogels, in this work we present a very different strategy, focused on enhancing the matrix-dominated properties of structural composites. Our approach has been to fill the space within continuous structural fibre-reinforced preforms with a porous carbon aerogel microstructure, to create a

hierarchical structural reinforcement, that can then be infused with resin. In this arrangement, the aerogel forms a bi-phasic reinforcement within the entire matrix-rich region, which can potentially support and promote load transfer between the fibres. The work was inspired by our previous studies into multifunctional (structural power) composites, which exploited the high surface area of CAG to generate significant electrochemical capacitance [18]. Although the focus of that work was to optimise electrochemical performance, an exciting observation was that the aerogel increased the modulus of the soft multifunctional matrix, and hence significantly enhanced the mechanical performance of the resulting composites. Specifically, we found that the in-plane shear modulus and strength increased 4.5-fold and by 52 %, respectively [18]. These enhancements suggest that CAG could improve the mechanical performance of traditional composites by stiffening the surrounding matrix, and hence supporting the fibres against lateral deformation. Therefore, in this study, a much broader range of other critical mechanical properties are investigated, including tension, compression, and interlaminar shear properties. In addition, some other physical properties are also reported, particularly through-thickness electrical and thermal conductivities, which are relevant to a number of applications, such as aircraft fuselage components [19].

2. Materials and methods

In this paper, all references to ‘aerogel’ relate to carbon aerogel based on resorcinol-formaldehyde (RF) pyrolysis [9]. The RF gels, unlike the conventional polymeric gels such as cross-linked polystyrene, are less affected by solvent exchanges. Initially, woven CF fabrics were infused with a RF precursor, which was aged at room temperature, 45 °C and 75 °C for 24 h at each temperature and left to cool to room temperature for around 4 h. The infused fabrics were then pyrolysed at 760 °C to produce a monolith CAG-infused CF preform. CAG composites were then produced by

infusing this preform with a non-structural polyethylene glycol diglycidyl ether (PEGDGE) matrix, known to exhibit good ionic conductivity [20] when combined with ionic liquid, but which is not in widespread use for structural applications due to its poor mechanical properties.

To investigate the feasibility of producing a composite that could viably be used for structural applications, the same process was used to reinforce a composite containing a conventional epoxy matrix. A resin system typically used in marine applications, namely Gurit PRIME 20LV [21], was selected for this purpose because of its good toughness and low viscosity, allowing rapid infusion into the CAG-reinforced CF fabrics. Evaluation of the performance of the CAG composites involved the measurement of the interlaminar shear strength (ILSS) and compression modulus and strength. Physical tests were conducted to characterise the specific surface area (SSA), and electrical and thermal conductivities of the composites. These results provide an indication of the expected electrical performance as a structural supercapacitor and in other contexts, such as lightning strike resistance. Scanning electron microscopy (SEM) of composites both without and with CAG was used to understand the relationship between the microstructure and mechanical properties, and to establish the dominant failure processes.

Subsequently, a comprehensive set of supplementary mechanical tests were performed on materials produced using only the structural PRIME 20LV matrix. These supplementary tests aimed to investigate the influence of the pyrolysis step on the parent fibres. Baseline composites containing as-received CF, control composites containing thermally-desized CF, and CF-CAG composites were fabricated, and the same test methods (longitudinal compression and interlaminar shear) were repeated,

along with additional longitudinal tensile tests. Comprehensive details regarding all the materials and methods are provided in the Electronic Supplementary Information (ESI).

This study investigated four composites: two reinforcements (with and without CAG) and two matrices (structural and multifunctional). The first two composites (multifunctional) were as-received CF and CF-CAG both infused with a PEGDGE (M_n ~ 526) matrix, with a triethylenetetramine (TETA, molar ratio of PEGDGE:TETA, 3:1) cross-linker, cured at 80 °C for 24 h. The third and fourth composites (structural) were as-received CF and CF-CAG, both infused with Gurit PRIME 20LV [21]. The laminates were cured at ambient for 24 h and then at 50 °C for 16 h as directed [21]. All the composites used HTA 3K 200 g/m^2 plain weave CF fabrics (Toho Tenax Europe GmbH woven by Tissa Glasweberei AG, Switzerland) laid up manually. Details of the properties of the as-received materials, laminate dimensions, stacking sequences and tests performed are provided in the ESI (Table S1). Throughout this paper, the PEGDGE-based composites without and with CAG are referred to as PEGDGE and CAG PEGDGE composites respectively, whilst those infused with the Gurit PRIME 20LV epoxy are referred to as PRIME and CAG PRIME composites. Scanning electron microscopy demonstrated the monolithic, mesoporous CAG network was homogeneous, surrounding the carbon fibres throughout the microstructure (Figure 1). The polymer resins infused throughout the pore volume of the CAG to complete a dense, bi-phasic, hierarchical matrix system.

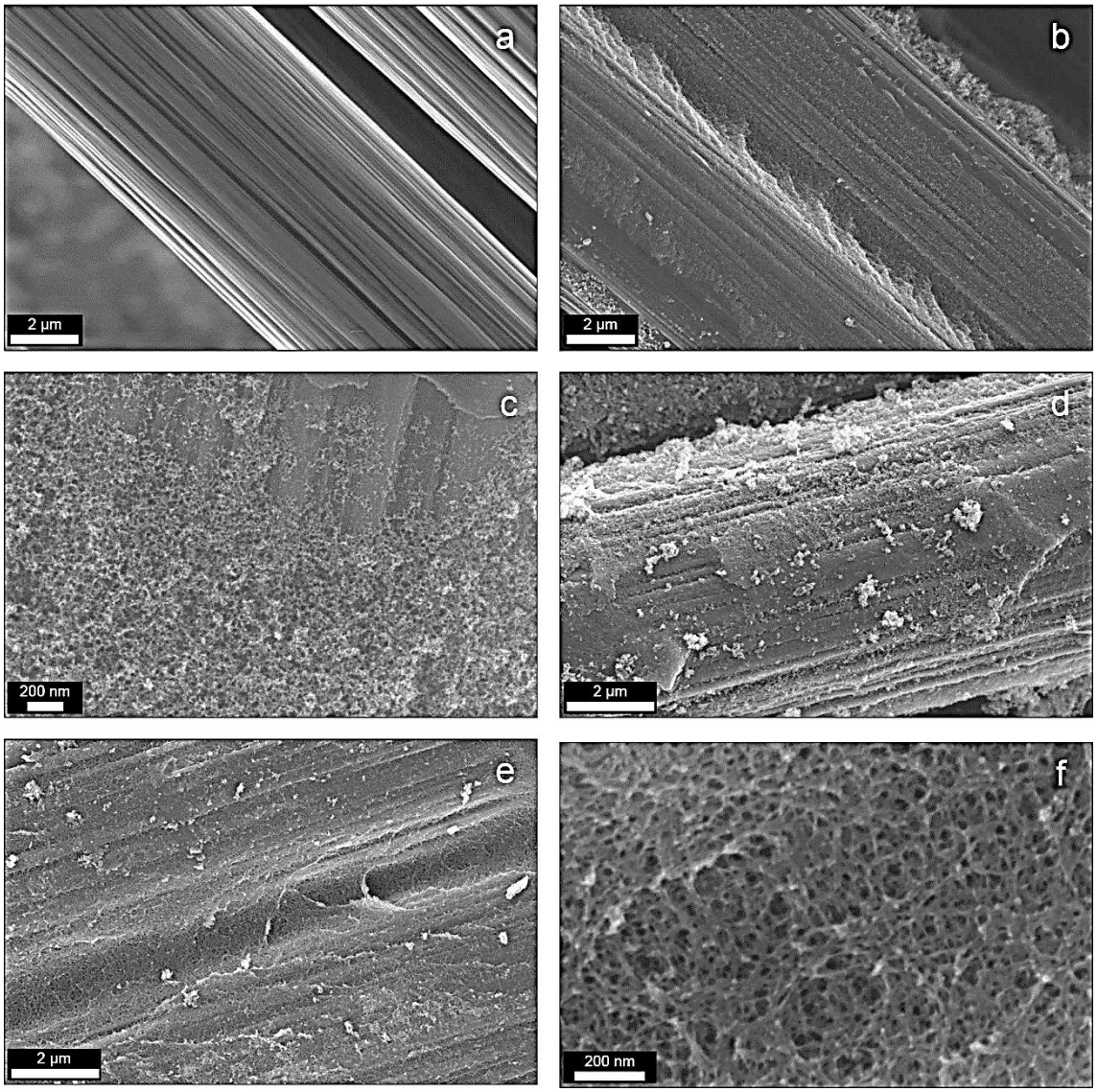

Figure 1 Scanning electron micrographs of (a) as-received, (b) - (d) CAG-CFs, (e)-(f) CAG between the CFs.

3. Mechanical characteristics

The short beam shear load-displacement curves for the PEGDGE and PRIME systems show different ranges due to the intrinsic moduli of the resin (Figure 2). The load-displacement response for the PEGDGE composite was linear until probable yielding of the PEGDGE matrix or fibre/matrix interface at just below 0.2 mm displacement (Figure 2a). Within the displacement range tested, there was no load drop

associated with the onset of interlaminar failure. However, the CAG PEGDGE, PRIME and CAG PRIME (Figure 2b) composites exhibited a peak load and a subsequent sharp drop, which follows the usual response [22] for a structural CFRP. The pure PEGDGE case (Figure 2a) shows no load drop, as the matrix is extremely compliant, behaving more like an elastomer and yielding without interlaminar fracture in the relevant displacement range. Since the PEGDGE system presented no clear yield point or load drop, an apparent ILSS was calculated using the point of transition from elastic to plastic deformation. This transition point was the intersection of two tangents to the curve just before and after the first reduction in slope. The reasoning for these observations is discussed after presenting optical cross-sections and scanning electron micrographs of the fracture surfaces.

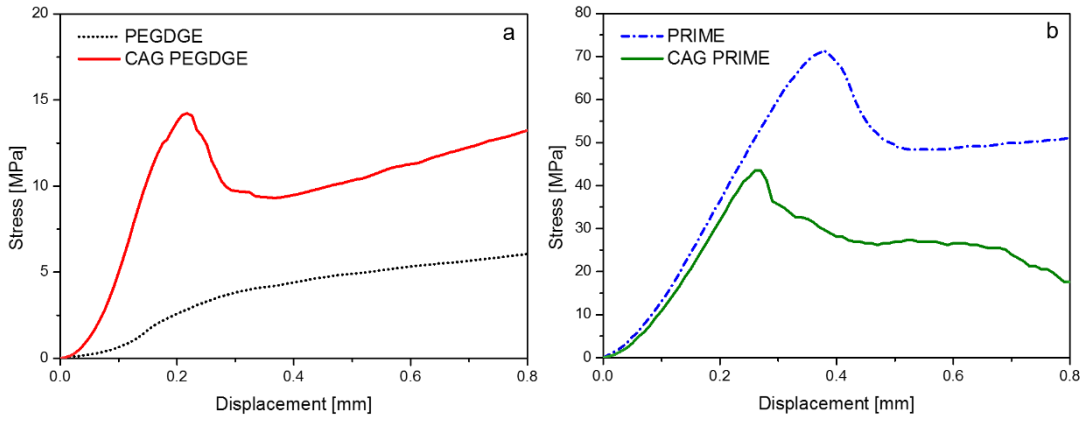

Figure 2 Representative stress–displacement curves for ILSS tests for composites with (a) PEGDGE-based and (b) PRIME epoxy matrix with and without CAG reinforcement.

For the PEGDGE composites, the ILSS increased by 312 % upon introducing CAG (Table 1), whilst for the stiffer PRIME composites, CAG reduced the ILSS by 29% (Table 1) without greatly affecting the slope of the response. Where appropriate, mechanical properties were also normalised by fibre volume fraction (V_f) to account for differences in composition (for predominately fibre-dominated properties). The CAG

volume fraction (V_a) is considered as part of the matrix phase, since the CAG combines with the resin to form the matrix system. In fact, V_f effects are not significant (differing by only 0.2% and 2.6%, for the PRIME and PEGDGE systems, respectively), compared to the dramatic changes in elastic modulus (e.g. almost four-fold for the PEGDGE system, both with and without v_f normalisation). The matrix volume fraction (V_m) is controlled by the available pore volume in the CAG microstructure; the reproducibility of resin infusion was demonstrated by the consistency of the PRIME composites manufactured in two completely independent series of experiments that yielded near identical average V_f values (56.5% and 55.3% respectively in Table 1).

Table 1 Fibre, matrix and aerogel volume fractions, ILSS, compressive moduli (E_c) and strengths (X_c) of PEGDGE- and PRIME-based composites.

Subscripts: f = fibres, m = matrix, a = aerogel, * normalised to 55 % V_f.

Fabric	Polymer	V_f (%)	V_m (%)	V_a (%)	ILSS (MPa)	X_c (MPa)	E_c (GPa)	E_c* (GPa)
CF	PEGDGE	57.1	42.9	-	3.4 ± 0.1	50.4 ± 3.8	16.6 ± 1.5	16.0 ± 1.5
CF-CAG	PEGDGE	55.7	38.9	5.4	14.0 ± 0.4	174.8 ± 9.2	60.5 ± 3.6	59.7 ± 3.6
CF	PRIME	56.3	43.7	-	60.5 ± 1.9	535.7 ± 52.2	65.4 ± 5.1	63.9 ± 5.1
CF-CAG	PRIME	56.5	38.5	5.0	43.0 ± 1.1	345.2 ± 29.2	80.6 ± 4.5	78.5 ± 4.5

Optical microscopy of polished sections of the failed specimens (Figure 3) showed no intralaminar cracks in the soft PEGDGE system, whilst the more brittle CAG PEGDGE system did display such cracking. In the PRIME composites, some

delaminations (or intrabundle cracks) were observed to branch off from matrix cracks, which must have formed first. There was no cracking in the conventional PRIME system even though it had experienced a higher load, consistent with a lower intralaminar performance in the CAG PRIME composite.

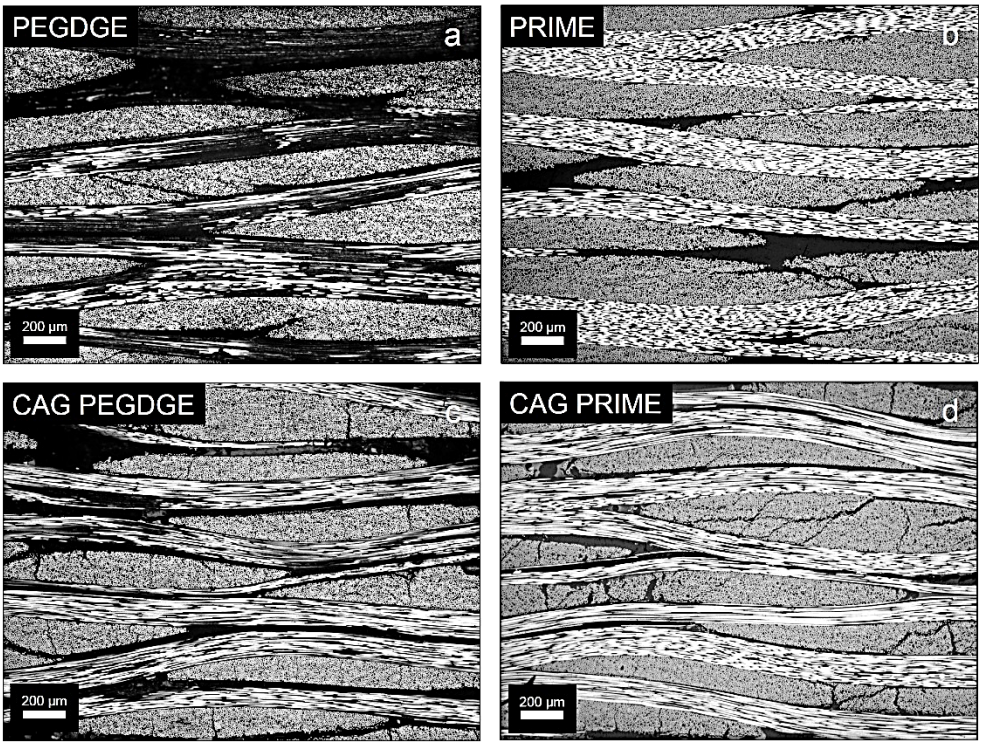

Figure 3 Observed damage in cross-sections of the tested ILSS composite specimens.

Scanning electron micrographs were taken at the mid-plane of the ILSS specimens to provide a comparison between the failure mechanisms (Figure 4). PEGDGE ILSS specimens without CAG exhibited small, regularly spaced cusps [23]. A good fibre/matrix interface was apparent from the presence of tufted feet on these cusps [23]. For the CAG PEGDGE, the fibres appeared slightly stripped of matrix, implying a poorer fibre/matrix interface, whilst the cusps were larger and more block-like, indicative of a thicker interply resin layer and inferior fibre/matrix interface [24].

Cusps were observed in both the PRIME and CAG PRIME composites (Figure 4), but there were smoother fibre imprints in the CAG PRIME specimens. Furthermore, in the CAG PRIME, the cusps were more block-like and had fewer tufted feet features than that in the PRIME system, again consistent with a poorer fibre/matrix interface [23]. Additionally, more interlaminar voids were present in the CAG PRIME, which would have also lowered the shear strength. Overall, the CAG PRIME composites had presented a poorer fibre/matrix interface.

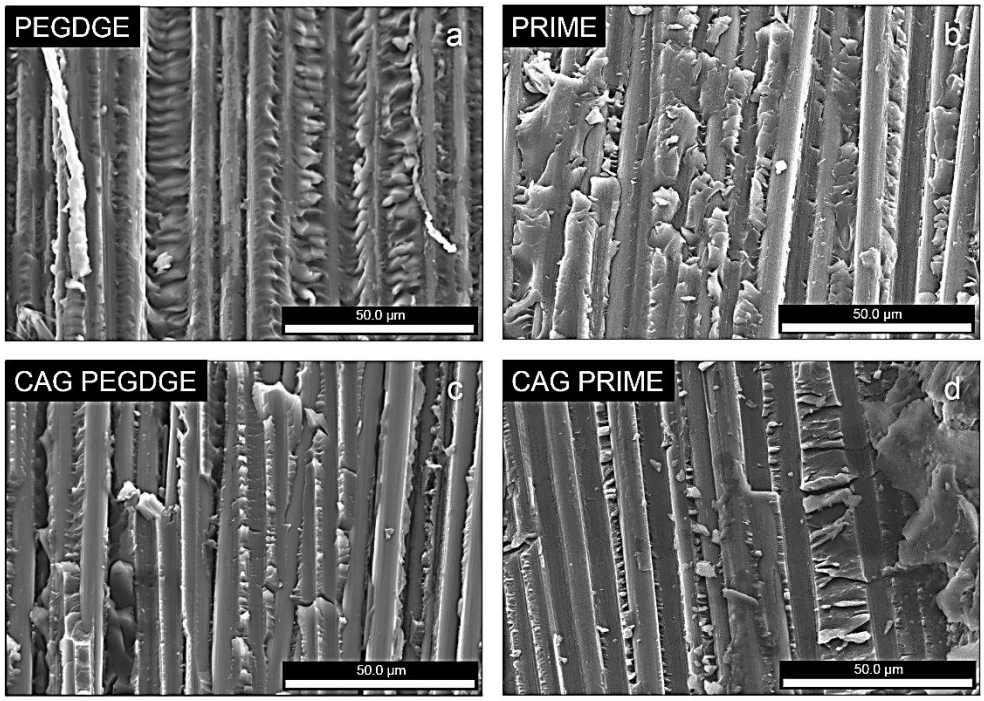

Figure 4 Fracture surfaces of the ILSS composite specimens.

Compression loading of the pure PEGDGE composite (Figure 5a) showed a progressive softening, whilst the CAG PEGDGE composite maintained a predominantly linear stress-strain response. For the CAG PEGDGE, three changes in slope were observed, highlighting the complexity of the response of this hierarchical material

system. These slope changes may have been caused by local buckling of the woven tows due to the low lateral support provided by the soft PEGDGE matrix, or by foam-like buckling of the rigid CAG struts. It should be noted that, due to variations in the V_f, the fibre-dominated properties were normalised by fibre volume fraction. In the PEDGDE system, the introduction of CAG increased the normalized compressive modulus by 273% and the compressive strength by 247% (Table 1).

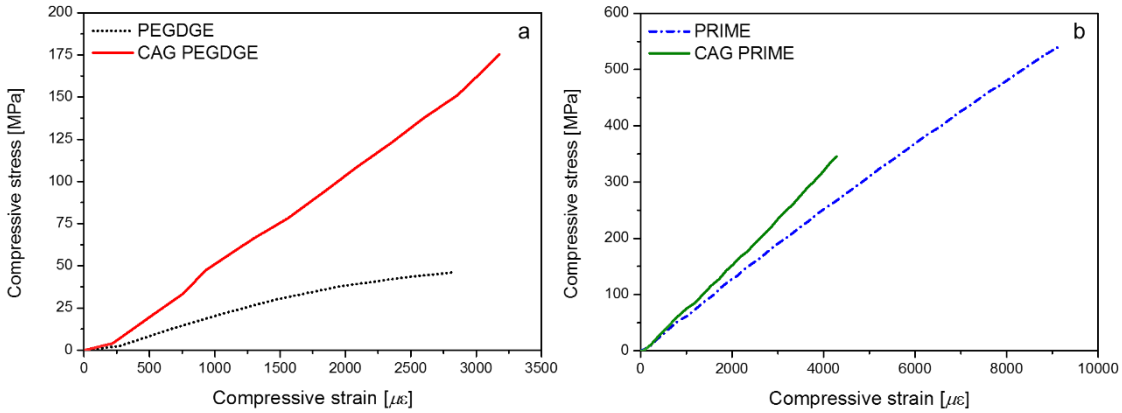

Figure 5 Representative compressive stress-strain curves for composites with (a) PEGDGE-based and (b) PRIME epoxy matrices.

For the PRIME composites (Figure 5b), similar stress-strain behaviour was observed, i.e. a reduction in slope with increasing strain for the pure PRIME composite and a linear stress-strain curve for the CAG PRIME composite. The baseline PRIME curve exhibited some non-linearity, likely associated with the matrix-dominated response of the transverse tows [25]. Some differences were observed between the front and back strain gauge responses, which indicated that the strengths determined were lower bounds on the actual compressive strengths. The addition of CAG increased the normalized compressive modulus by 23% but the compressive strength dropped by 36% (Table 1).

Different fracture modes were evident from examination of the failed compression specimens (Figure 6). The PEGDGE composites displayed a ‘green stick’ type fracture [26], presenting extensive delamination but no fibre fractures, as expected for a soft matrix. However, the CAG PEGDGE specimens presented localised fibre fractures in the form of micro-buckling failures with very limited delamination.

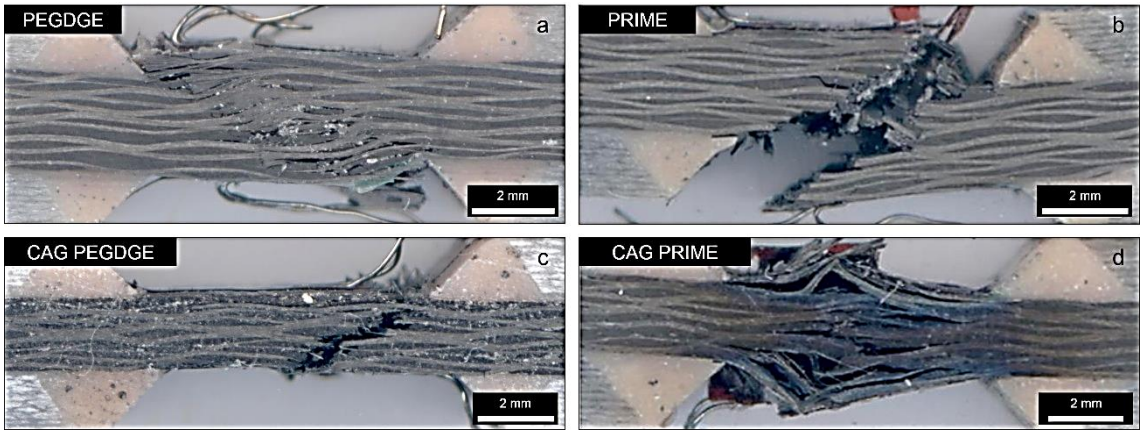

Figure 6 Edges of representative compression specimens for PEGDGE and PRIME based composites, without and with CAG.

For the PRIME composites, the introduction of the CAG led to the opposite trend in the fracture processes. The baseline PRIME composite had a localised microbuckling failure, but with CAG, delaminations had developed prior to compressive microbuckling. From the continuity of the fracture surfaces, it was apparent that the exterior layers had delaminated first, with only localised fibre fractures in the interior, which was consistent with the lower ILSS of the CAG PRIME composites.

Hierarchical composite compression properties are expected to be improved through the addition of CNTs or other discrete nanoreinforcements within the matrix, as

they have higher moduli and shear strengths [27] than un-reinforced epoxy matrix systems. For example, by adding 10 wt% CNTs to CFRPs, the compression modulus has been found to increase by 6.7% (from 47.0 to 50.2 GPa) and the compression strength increased by 14% (from 447 to 511 MPa) [28]. However, it should be noted that a significant modulus enhancement is not expected in such hierarchical systems, as the main reinforcement (often CF) modulus is orders of magnitude greater than polymer-reinforced nanocomposites, even for high CNT loading fractions [29]. For example, an increase in compressive strength of up to 39% (from 560 to 780 MPa) has also been reported with the addition of 0.5 wt.% CNTs [30], with no change in the compressive modulus. An improved compression strength is observed in discrete nanoreinforced hierarchical composites as the main failure mode of shear driven and kink-band formations [31], is delayed due to local lateral stiffening. Compared to CNT reinforcement, the CAG reinforcement presented in this work offered better relative mechanical performance improvements for the PEGDGE matrix which had intrinsically low mechanical properties, but not for the PRIME matrix system, which has higher intrinsic modulus and strength. The explanation for this is thought to be caused by thermal desizing during the CAG synthesis process, which is presented in the next Section.

3.1 Effect of thermal desizing

A key question arising from the results was why, after CAG modification, all the mechanical properties had improved for the PEGDGE composites, but only the modulus had marginally improved for the PRIME composites. One possible explanation was that the CAG/PRIME interfaces and/or the heat-treated CF/PRIME interfaces and/or the CF/CAG interfaces were relatively weak compared to the matrix, either intrinsically or

due to the removal of fibre sizing during processing. Additional work on the PRIME system extended the range of mechanical data and provided further details of changes in the fibre-matrix interface, during processing. Composites based on both the conventional and CAG systems were compared to controls reinforced with carbon fibres heated at the CAG production temperature of 760 °C. This heating step reduced the ILSS of a control composite based on CF alone by 35 %; a similar drop to that observed for the subsequent CAG samples (Table 2), suggesting a common mechanism. Numerous cusps and a highly textured matrix were seen in the electron micrographs of the PRIME baseline ILSS specimens (Figure 7a,b), consistent with a relatively good fibre/matrix adhesion [23].

Table 2 Mechanical properties of additional PRIME matrix composites tested to understand the influence of processing on mechanical performance. Symbols: E = Young's modulus, X = longitudinal strength.

Subscripts: f = fibres, c = compressive, t = tensile, * normalised to 55 % V_f.

	V_f (%)	ILSS (MPa)	E_c (GPa)	E_c* (GPa)	X_c (MPa)	E_t (GPa)	E_t* (GPa)	X_t (MPa)
Baseline	54.4	55.9 ±0.3	62.0 ±1.0	62.7 ±1.0	634.6 ±16.2	62.6 ±0.7	63.3 ±0.7	813.2 ±4.3
Thermally -desized	56.1	36.0 ±1.2	60.3 ±0.5	59.1 ±0.5	453.1 ±17.1	64.8 ±0.7	63.5 ±0.7	729.5 ±22.1
CAG	55.3	37.1 ±0.5	63.9 ±0.5	63.6 ±0.5	331.2 ±9.3	65.3 ±0.5	64.9 ±0.5	409.0 ±7.1

** normalised to 55 % V_f*

In the thermally-desized specimen (Figure 7b), eye-shaped splits were observed in the fibre tracks in the matrix (left hand side), indicative of very poor bonding at the fibre/matrix interface [23]. The loss of interfacial adhesion may have been due to the thermal decomposition [32] of the surface oxides [33] on the CFs or the removal of the size [34]. For the CAG specimen (Figure 7c), the fibre imprints were smoother than those in the baseline (Figure 7a), but it was difficult to infer the toughness of the interface from the morphology of the matrix due to the uncertain influence of the CAG on this textured microstructure.

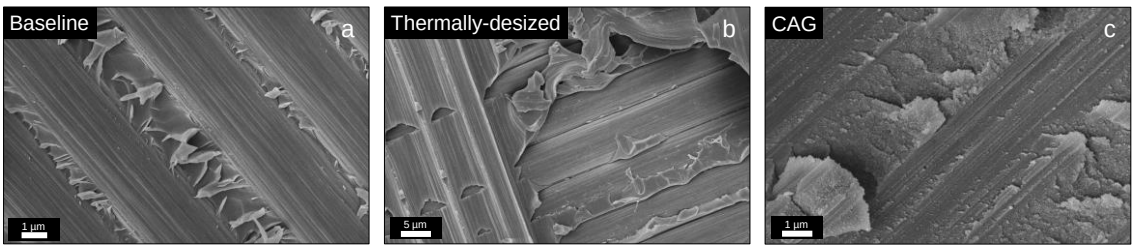

Figure 7 Scanning electron micrographs of fracture surfaces of the ILSS specimens.

The baseline, thermally-desized and CAG composites all presented similar tensile moduli (Table 2), indicating that the processing and CAG synthesis [35] had not altered the fibre microstructure or led to damage in the fibre cores [36]. However, there was a 5.7% reduction in normalised compressive modulus after pyrolysis of the control samples (Table 2), which was attributed to damage to the fibre-matrix interface. After the loss of surface oxides and/or size, the fibres were more difficult to handle during lay-up before resin infusion, increasing the likelihood of misalignment. However, the RF-infused CF laminates were rigid after aging and no such handling issues occurred in the case of the CAG composites. Misalignment of the fibres was more critical in

compression than in tension tests, which explains why the tensile moduli were not significantly influenced by the size removal.

There were significant reductions in both tensile and compressive strengths (Table 2) of 10% and 50% for the thermally-desized and CAG PRIME composites respectively compared to those of the baseline. Since pyrolysis removed the fibre sizing and led to surface oxidation [37], a reduction in fibre and fibre-matrix interface [38] quality and hence a decrease in tensile strength was anticipated. The greater reduction in the case of the introduction of CAG might reflect damage to the CF microstructure by residual water/methanol in the CAG precursor during pyrolysis [39]. However, the increase in performance of the CAG PEGDGE over the PEDGDE system suggested the lower performance of the CAG PRIME was primarily related to an interfacial issue rather than degradation of the fibres themselves.

Overall, two different mechanisms were thought to contributed to the lowering of these strengths. The elevated temperatures in pyrolysis would have led firstly to removal of the sizing and secondly to the loss of functional groups on the fibre surface, thereby weakening the fibre-matrix interface and its ability to transfer load effectively.

3.2 Fractographic analysis

The fracture surfaces of the baseline composites are shown in Figure 8a,b. The failure morphology in the baseline was typical of compression failure, presenting microbuckled fibres (Figure 8a). In this baseline, the matrix had strongly adhered to the fibres (Figure 8b) enabling higher compressive stresses to be achieved before failure. In the thermally-desized composite (Figure 8c,d), cleaner fibres were apparent, attributed to a poor fibre/matrix interface, which would have reduced the lateral support from the matrix on the fibres.

In the CAG composite (Figure 8e,f), the splitting between the failed tows was more extensive (Figure 8e, top: 90° ply split, bottom: 0° ply split) than that in the baseline and thermally-desized samples, which would have promoted delamination initiation. The delaminated fracture surfaces presented a thick layer of matrix covering the carbon fibres and smooth fibre tracks (Figure 8e), which was consistent with interfacial rather than cohesive fracture of the matrix. This suggested the interface strength was not enough to support the fibres against microbuckling and therefore resulted in a reduced compression strength.

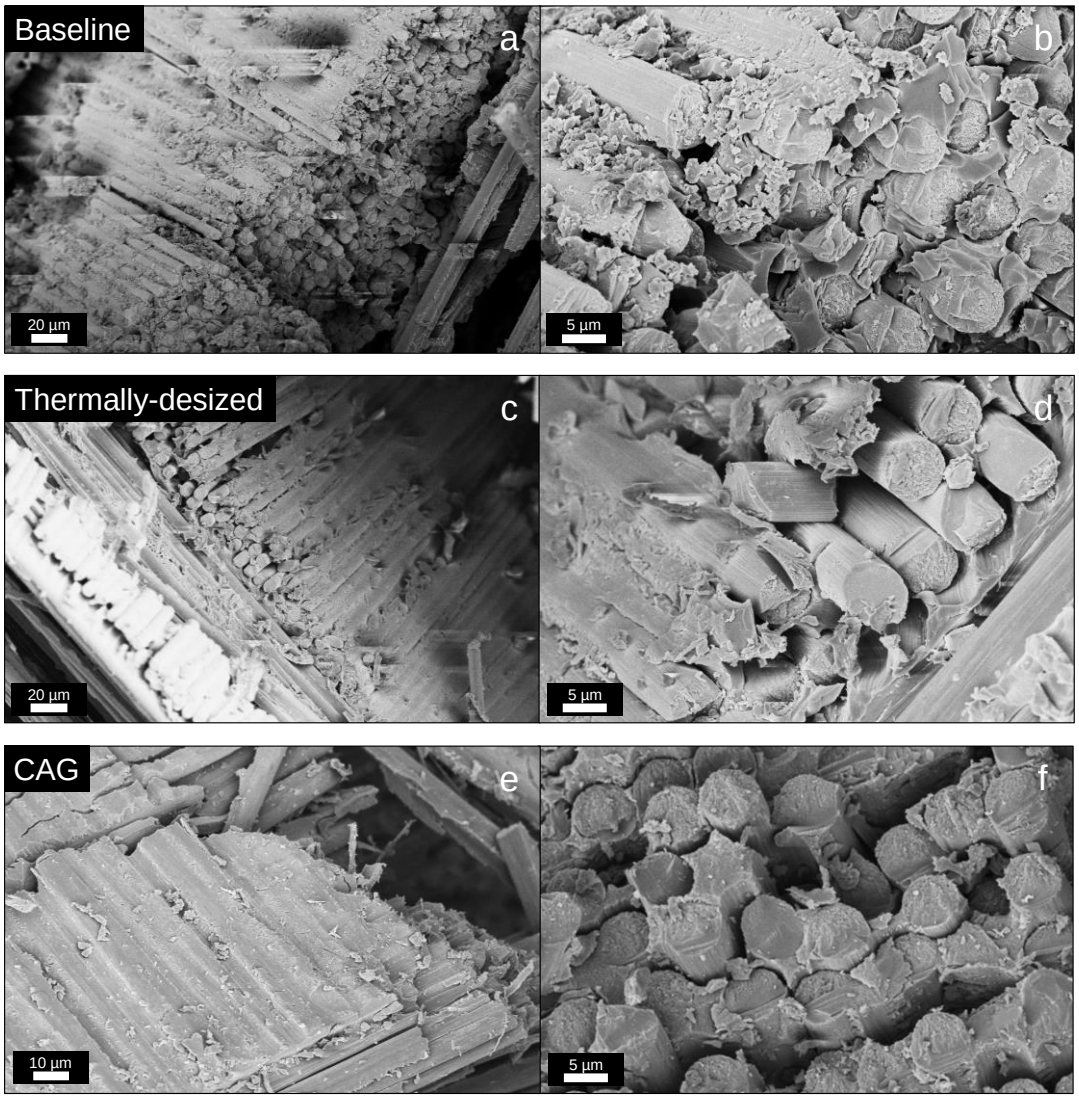

Figure 8 Fracture surfaces in the (a, b) baseline, (c, d) thermally-desized and (e, f) CAG composite compression specimens.

If the interface between the fibres and the hierarchical CAG/polymer matrix could be improved, then premature interfacial failure which led to microbuckling could be suppressed, since the stiffer bi-continuous CAG-matrix can support the fibres more effectively than a conventional resin. In principle, post treatment of the monolithic CAG-fibre preforms [40] before matrix infusion could be undertaken to recover the lost fibre surface functionalization though various methods including acid treatments [18], electrochemical [41] or gas phase functionalization [42].

4. Physical characteristics

The thermal and electrical properties of the baseline, thermally-desized and CAG PRIME composites are presented in Table 3. The glass transition temperatures (T_g) for all the samples were in the range from 93 to 102 °C, slightly higher than the value reported by the manufacturer [21]. There was no significant change in T_g on introducing CAG, however, the thermally-desized composite exhibited a slightly lower T_g when compared to that of the baseline, attributed to the weak fibre/matrix interface and loss of interfacial functionalization [43].

The in-plane electrical conductivities of the baseline and the thermally-desized/CAG samples (Table 3) were not significantly different, since, in this orientation, the conductivity was dominated by the CF fabric. However, the out-of-plane electrical conductivity increased in both the thermally-desized and CAG samples by 92% and 118%, respectively. This increase could be attributed to poorer infiltration of the resin leading to greater fibre contact.

The additional improvement in electrical conductivity for the CAG over the thermally-desized sample was attributed to the inclusion of the electrically conductive CAG network in the composite. For the CAG sample, the total carbon content was 6

wt.% higher than that of the thermally-desized sample, which led to a 14% relative increase in out-of-plane electrical conductivity. However, it should be noted that amorphous carbon has lower intrinsic electrical conductivity than graphitised CF [44].

The introduction of CAG increased the out-of-plane thermal diffusivity in composites by 25% compared that of the baseline. The large uncertainty in specific heat capacity makes it difficult to draw firm conclusions about thermal conductivity, although it appears to have been similar for all samples (ca. 1.7 W/mK, Table 3). The CAG component might be expected to increase thermal conductivity, but nanostructured fillers are known to offer limited benefits in this context due to the large fraction of interfaces with high thermal resistance [45]; a reduced polymeric fraction would be expected to reduce heat capacity.

Table 3 Physical properties of PRIME composites. D = out-of-plane thermal diffusivity, c_p = specific heat capacity. k = thermal conductivity, σ = electrical conductivity.

	T_g	D	c_p	k	σ (S/m)	
	(°C)	(mm^2/ms)	(J/g-K)	(W/m-K)	In-plane	Out-of-plane
Baseline	101.8 ± 3.0	487 ± 5	2.48 ± 0.30	1.8 ± 0.2	2307 ± 664	8.4 ± 1.4
Thermally-desized	93.9 ± 1.0	514 ± 7	2.06 ± 0.25	1.6 ± 0.2	3007 ± 840	16.1 ± 2.1
CAG	100.3 ± 2.5	609 ± 10	1.82 ± 0.04	1.7 ± 0.1	2224 ± 443	18.3 ± 3.2

5. Concluding remarks

Carbon aerogel-reinforced CFRPs were fabricated using a reliable and scalable RIFT process and characterised to assess the performance of CAG as a hierarchical matrix reinforcement to support continuous fibres in structural composites. A porous,

bicontinuous CAG microstructure (6.5 wt.% loading) was formed uniformly around the CFs and successfully infused with secondary, polymer-based resin, to form a nanostructured matrix system. The intrinsic performance of this 'matrix' is hard to determine, due to the difficulties of preparing pure CAG monoliths without a fibre support, as noted in the introduction, but it clearly strongly influences the performance of the resulting composites. Further improvements might be obtained by optimising or reinforcing the CAG nanostructure, for example with other nanocarbons [13].

Multifunctional PEGDGE matrix composites presented improved ILSS, compressive stiffness and compressive strength with CAG reinforcement. Although the mechanical performance using this matrix system was too modest for use in primary structural applications, CAG did provide considerable benefits both in mechanical properties and electrical performance, relevant to multifunctional applications.

CAG reinforcement of CFRPs containing a structural PRIME 20ULV matrix had no major influence on the tensile and compressive modulus. However, the strengths reduced (on average) under interlaminar shear by 34%, under compression by 42% and under tension by 50%. Based on the mechanical test results and fractographic analysis, the CAG reinforcement process appeared to have weakened the fibre/matrix interfaces. Both the thermally-desized and CAG-reinforced composites presented similar values of ILSS, suggesting that the removal of fibre sizing and hence poor fibre/matrix interfacial adhesion resulted from the processing method used to produce the CAG.

The CAG-reinforced composites developed here would be suitable for stiffness driven applications, where low density is important. Beyond this study, there are promising prospects for improving the interfacial characteristics in these hierarchical composites, potentially leading to an improvement in compression strength. The carbon surfaces of the CAG-CF could be functionalised after aerogel carbonisation to

regenerate functional groups compatible with the subsequent resin infusion. A particularly promising approach may be to use a clean, versatile, self-limiting gas phase chemistry [33]. If high temperature CAG processing proves to be a significant obstacle, other classes of rigid aerogel could be considered to limit any potential degradation of the primary fibre characteristics. Further work will be devoted to lower temperature processing routes to achieve the mechanical and electrical benefits offered by CAG reinforcement without compromising the fibre/matrix interface adhesion.

In conclusion, this research has demonstrated that a completely new approach of using hierarchical CAG-reinforced CFRPs represents a potential route to addressing the issue of poor matrix-dominated properties.

Acknowledgements

The authors kindly acknowledge the funding for this research provided by Defence Science and Technology Laboratory under MAST 2.2.2, and EPSRC programme Grant EP/I02946X/1 on High Performance Ductile Composite Technology, in collaboration with the University of Bristol, Beyond structural - Multifunctional composites that store electrical energy (EP/P007465/1) and Structural pOweR CompositEs foR futurE civil aiRcraft (SORCERER) Project funded by EU Horizon 2020 Programme (H2020-EU.3.4.5.1. #738085) which is part of the Clean Sky 2 Funding Scheme (CS2-RIA - Research and Innovation action). Appreciation is also expressed to Tomi Herceg for testing the DSC and DMTA samples and INDSPEC Chem. Corp for providing RF resin. S. Nguyen and D. B. Anthony contributed equally to this work.

References

[1] Y. Martinez-Rubi, et al., Toughening of Epoxy Matrices with Reduced Single-Walled Carbon Nanotubes, ACS Applied Materials & Interfaces 3(7) (2011) 2309-2317.

[2] H. Qian, et al., Carbon nanotube-based hierarchical composites: a review, Journal of Materials Chemistry 20(23) (2010) 4751-4762.

[3] F. Yavari et al., Dramatic Increase in Fatigue Life in Hierarchical Graphene Composites. ACS Applied Materials & Interfaces 2(10) (2010) 2738–2743.

[4] L. Gorbatikh et al., Hierarchical design of structural composite materials down to the nanoscale via experimentation and modelling. IOP Conference Series: Materials Science and Engineering 406(012002) (2018) 1-6.

[5] D.B. Anthony et al., Continuous Carbon nanotube Synthesis On Charged Carbon Fibers. Composites Part A: Applied Science and Manufacturing 112 (2018) 525-538.

[6] J. Qiu, Carbon nanotube integrated multifunctional multiscale composites. Nanotechnology 18(275708) (2007) 1-11.

[7] T.M. Herceg, et al., Thermosetting hierarchical composites with high carbon nanotube loadings: En route to high performance, Composites Science and Technology 127 (2016) 134-141.

[8] G. Allegri, et al., A novel model of delamination bridging via Z-pins in composite laminates, International Journal of Solids and Structures 51(19) (2014) 3314-3332.

[9] R.W. Pekala, Organic aerogels from the polycondensation of resorcinol with formaldehyde, Journal of Materials Science 24(9) (1989) 3221-3227.

[10] T.H. Hsieh, Y.S. Huang, The mechanical properties and delamination of carbon fiber-reinforced polymer laminates modified with carbon aerogel, Journal of Materials Science 52(6) (2017) 3520-3534.

[11] T.-H. Hsieh, et al., Mechanical properties and toughness of carbon aerogel/epoxy polymer composites, Journal of Materials Science 50(8) (2015) 3258-3266.

[12] S. Chandrasekaran, et al., Fracture, failure and compression behaviour of a 3D interconnected carbon aerogel (Aerographite) epoxy composite, Composites Science and Technology 122 (2016) 50-58.

[13] A. Lamy-Mendes, et al., Advances in carbon nanostructure-silica aerogel composites: a review, Journal of Materials Chemistry A 6(4) (2018) 1340-1369.

[14] J. Feng, et al., Carbon Aerogel Composites Prepared by Ambient Drying and Using Oxidized Polyacrylonitrile Fibers as Reinforcements, ACS Applied Materials & Interfaces 3(12) (2011) 4796-4803.

[15] R. Fu, et al., Fabrication of Activated Carbon Fibers/Carbon Aerogels Composites by Gelation and Supercritical Drying in Isopropanol, Journal of Materials Research 18(12) (2003) 2765-2773.

[16] H. Cheng, et al., Preparation, mechanical, thermal and ablative properties of lightweight needled carbon fibre felt/phenolic resin aerogel composite with a bird's nest structure, Composites Science and Technology 140 (2017) 63-72.

[17] F.-L. Guan, et al., Fiber-reinforced three-dimensional graphene aerogels for electrically conductive epoxy composites with enhanced mechanical properties, Chinese Journal of Polymer Science 35(11) (2017) 1381-1390.

[18] H. Qian, et al., Multifunctional Structural Supercapacitor Composites Based on Carbon Aerogel Modified High Performance Carbon Fiber Fabric, ACS Applied Materials & Interfaces 5(13) (2013) 6113-6122.

[19] F. Moupfouma, et al., Electromagnetic Protection Hazards on Composite versus Metallic Aircraft, SAE International Journal of Aerospace 6(2) (2013).

[20] N. Shirshova, et al., Structural composite supercapacitors, 46 (2013) 96–107.

[21] Gurit, UK Ltd. PRIME 20ULV Ultra Low Viscosity Epoxy Infusion System Provisional Datasheet, Engineering Office, 9 South Point, Ensign Way, Hamble, SO31 4RF, UK, 2014.

[22] ASTM Standard D2344M - 13, Standard Test Method for Short-Beam Strength of Polymer Matrix Composite Materials and their Laminates, ASTM International, West Conshohocken, PA, 2013.

[23] E. Greenhalgh, Failure Analysis and Fractography of Polymer Composites, Woodhead Publishing2009.

[24] S. Singh, I.K. Partridge, Mixed-mode fracture in an interleaved carbon-fibre/epoxy composite, Composites Science and Technology 55(4) (1995) 319-327.

[25] N.V. De Carvalho, et al., An experimental study of failure initiation and propagation in 2D woven composites under compression, Composites Science and Technology 71(10) (2011) 1316.

[26] E.S. Greenhalgh, et al., Fractographic observations on Dyneema® composites under ballistic impact, Composites Part A: Applied Science and Manufacturing 44 (2013) 51-62.

[27] T Zhuo, et al., Study on Mechanical, Thermal and Electrical Characterizations of Nano-SiC/Epoxy Composites, Polymer Journal 2009;41:51–57.

[28] T. Iwahori, Y., et al., Mechanical properties improvements in two-phase and three-phase composites using carbon nano-fiber dispersed resin. Composites Part a-Applied Science and Manufacturing 2005;36(10):1430-39.

[29] T. Herceg, Nano and hierarchical composites with high CNT loading fractions, PhD Thesis, Imperial College London, 2013, uk.bl.ethos.669487.

[30] J. Cho, et al., Effects of block copolymer dispersant and nanotube length on reinforcement of carbon/epoxy composites. Composites Part A: Applied Science and Manufacturing 2008;39(12):1844-50.

[31] Gutkin, R., et al., On the transition from shear-driven fibre compressive failure to fibre kinking in notched CFRP laminates under longitudinal compression. Composites Science and Technology, 2010;70(8):1223-31.

[32] Z. Dai, et al., Effect of heat treatment on carbon fiber surface properties and fibers/epoxy interfacial adhesion, Applied Surface Science 257(20) (2011) 8457-8461.

[33] R. Verdejo, et al., Removal of oxidation debris from multi-walled carbon nanotubes, Chemical Communications (5) (2007) 513-515.

[34] J. Zhang, et al., Interfacial studies of carbon fiber/epoxy composites using single fiber fragmentation test, Composite Interfaces 20(6) (2013) 421-429.

[35] H. Qian, et al., Carbon nanotube grafted carbon fibres: A study of wetting and fibre fragmentation, Composites Part A: Applied Science and Manufacturing 41(9) (2010) 1107-1114.

[36] A.Y. Boroujeni, et al., Hybrid carbon nanotube–carbon fiber composites with improved in-plane mechanical properties, Composites Part B: Engineering 66 (2014) 475-483.

[37] B. Li, et al., Surface Oxidation of Carbon Fiber and its Influence on the Properties of Carbon Fiber Reinforced BN-Si 3 N 4 Composites, 2008.

[38] P. Mallick, Fiber-Reinforced Composites: Materials, Manufacturing, and Design, Third Edition ed., CRC Press, Taylor & Francis Group, LLC2007.

[39] J. Alcañiz-Monge, et al., Effect of the activating gas on tensile strength and pore structure of pitch-based carbon fibres, Carbon 32(7) (1994) 1277-1283.

[40] DB.Anthony, et al., Applying a potential difference to minimise damage to carbon fibres during carbon nanotube grafting by chemical vapour deposition. Nanotechnology 28(30) (2017) 305602.

[41] A.M. Pezeshki, et al., Elucidating effects of cell architecture, electrode material, and solution composition on overpotentials in redox flow batteries. Electrochimica Acta 229 (2017) 261-270.

[42 R. Menzel, et al., A versatile, solvent-free methodology for the functionalisation of carbon nanotubes. Chemical Science 1(5) (2010) 603-608.

[43] A. Bismarck, et al., Study on surface- and mechanical fiber characteristics and their effect on epoxy composite properties tuned by continuous anodic carbon fiber oxidation, Journal of Adhesion Science and Technology 14(5) (2000) 661-690.

[44] A.M. Kern, et al., Thermal and Electrical Conductivity of Amorphous and Graphitized Carbide-Derived Carbon Monoliths, Chemical Engineering & Technology 39(6) (2016) 1121-1129.

[45] A. Yu, et al., Enhanced Thermal Conductivity in a Hybrid Graphite Nanoplatelet – Carbon Nanotube Filler for Epoxy Composites, Advanced Materials 20(24) (2008) 4740-4744.

Figure captions

Figure 1 Scanning electron micrographs of (a) as-received, (b) - (d) CAG-CFs, (e)-(f) CAG between the CFs.

Figure 2 Representative stress–displacement curves in ILSS tests for composites with (a) PEGDGE-based and (b) PRIME epoxy matrix with and without CAG reinforcement.

Figure 3 Observed damage in cross-sections of the tested ILSS composite specimens.

Figure 4 Fracture surfaces of the ILSS composite specimens.

Figure 5 Representative compressive stress-strain curves for composites with (a) PEGDGE-based and (b) PRIME epoxy matrices.

Figure 6 Edges of representative compression specimens for PEGDGE and PRIME based composites, without and with CAG.

Figure 7 Scanning electron micrographs of fracture surfaces of the ILSS specimens.

Figure 8 Fracture surfaces in the (a, b) baseline, (c, d) thermally-desized and (e, f) CAG composite compression specimens.

Table captions

Table 1 Fibre, matrix and aerogel volume fractions, ILSS, compressive moduli (E_c) and strengths (X_c). Subscripts: f = fibres, m = matrix, a = aerogel, * normalised to 55 % V_f.

Table 2 Mechanical properties of PRIME matrix composites tested to understand the influence of processing on mechanical performance. Symbols: E = Young's modulus, X = longitudinal strength. Subscripts: f = fibres, c = compressive, t = tensile, * normalised to 55 % V_f.

Table 3 Thermal and electrical properties of PRIME matrix composites. D = out-of-plane thermal diffusivity, c_p = specific heat capacity. k = thermal conductivity, σ = electrical conductivity.